

Hydrothermal synthesis of nanocrystalline hydroxyapatite from phosphogypsum waste

Hiba Bensalah^{a,b,*}, Maged F. Bekheet^b, Saad Alami Younssi^a, Mohamed Ouammou^a, Aleksander Gurlo^b

^a Laboratory of Membranes, Materials and Environment, Department of Chemistry, Faculty of Sciences & Technics of Mohammedia BP 146, 20650, University Hassan II of Casablanca, Morocco

^b Fachgebiet Keramische Werkstoffe, Institut für Werkstoffwissenschaften und-technologien, Technische Universität Berlin, Hardenbergstraße 40, 10623 Berlin, Germany



ARTICLE INFO

Keywords:

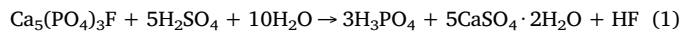
Phosphogypsum
Hydroxyapatite
Nanorods
Hydrothermal
Surfactant

ABSTRACT

Hydroxyapatite (HAp) nanorods are synthesized from phosphogypsum waste (PG) and potassium dihydrogen phosphate (KH_2PO_4) under hydrothermal conditions. The influence of several synthesis parameters such as temperature (100–200 °C), synthesis time (1–15 h), and solution pH (5–11) on product structure and purity is addressed by X-ray diffraction and Fourier Transformed-Infrared Spectroscopy. Phase-pure HAp nanorods with diameter and length of 18 and 63 nm, respectively, are obtained after 10 h at 200 °C and pH ~ 11. The influence of Brij-93 surfactant on the morphology of prepared HAp is investigated by transmission and scanning electron microscopy. The aspect ratio and the mean size of HAp crystals increase to 1013 and 205 × 20 nm, respectively, with increasing the concentration of Brij-93 surfactant to 0.01 mol. Hence, the PG recycling could be accomplished using an easy synthesis route with relatively cheap reactants for the production of nanocrystalline HAp.

1. Introduction

Phosphogypsum (PG) is an industrial waste appeared from the production of phosphoric acid where the phosphate ore is dissolved in sulfuric acid [1]:



About 5 tons of phosphogypsum are produced for every ton of P_2O_5 manufactured [2]. Worldwide PG production is huge, and it is estimated that 280 million tons are produced annually in phosphoric acid plants [3]. Until now, only 15% of world PG production is recycled as building materials, agricultural fertilizers or soil stabilization amendments and as setting regulator instead of natural gypsum in the Portland cement industry [4–6]. In fact, 85% of the worldwide production remains at present stored into piles near the factory that occupy considerable land resources, or completely discharged into water, which lead to serious contamination [2]. In consequence, valorizing and minimizing the negative effects of this waste increasingly grab the attention of researchers all around the world.

Since hydroxyapatite ($\text{Ca}_{10}(\text{PO}_4)_6(\text{OH})_2$, HAp) is the major mineral constituent of human hard tissues such as bones and teeth, synthetic

hydroxyapatite has received large attention as bone and teeth implants [7,8]. HAp has been extensively used also as a catalyst [9–12], catalyst support [13,14], biosensor [15–17] and adsorbent for several heavy elements, organic dyes and fluoride ions [18–21]. Recent studies showed that the nanostructured HAp exhibits multi-adsorbing sites, large surface area, and high biocompatibility [8,17,22]. In enamel HAp is present as highly crystalline nanorods with length and diameter of 100–1000 nm and 33–65 nm, respectively [23,24]. Thus, the synthesis of nanosized HAp materials with control over size and morphology of crystals is essential for a variety of applications. HAp was previously synthesized by various methods such as solid-state reaction [25], coprecipitation [7], sol-gel process [26], hydrothermal methods [22,27], and microwave synthesis route [21]. Some of these synthesis techniques have some drawbacks such as long reaction times, agglomeration, uncontrolled particle size and non-stoichiometric products. Among all these synthesis methods, the hydrothermal method, that can combine moderate temperatures with high pressures, is often used to prepare nanocrystalline HAp with controlled size and morphology [22,27]. Moreover, as surfactants are found to be the best shape directing agents allowing control over size and morphology of nanocrystals [28], they have also been explored in the HAp synthesis. For example, Wang et al.

Abbreviations: PG, phosphogypsum; HAp, hydroxyapatite

* Corresponding author at: Laboratory of Membranes, Materials and Environment, Department of Chemistry, Faculty of Sciences & Technics of Mohammedia BP 146, 20650, University Hassan II of Casablanca, Morocco.

E-mail address: hiba.bensalah@ceramics.tu-berlin.de (H. Bensalah).

<https://doi.org/10.1016/j.jece.2018.01.052>

Received 2 August 2017; Received in revised form 11 December 2017; Accepted 25 January 2018

Available online 16 March 2018

2213-3437/ © 2018 Elsevier Ltd. All rights reserved.

succeeded to regulate the growth of HAp crystals by the addition of cationic surfactant hexadecyltrimethylammonium bromide (CTAB) [22].

Accordingly, the aim of this work is to convert industrial waste PG into nanocrystalline HAp and to achieve control over the size and morphology of the HAp crystals by applying surfactant-assisted hydrothermal technique. A nonionic Brij-93 ($C_{18}H_{35}(OCH_2CH_2)_2OH$) surfactant, containing polar polyoxyethylene groups separated by hydrophobic polyethylene chain, is applied in this study. The influence of pH, temperature, time and surfactant concentrations on the structure and composition of HAp formed in a hydrothermal process are investigated by X-ray diffraction (XRD), Fourier Transformed-Infrared Spectroscopy (FTIR), scanning (SEM) and transmission electron microscopy (TEM).

2. Experimental

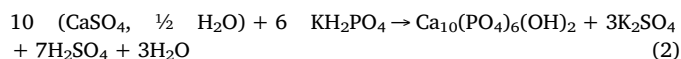
2.1. Materials

The phosphogypsum (PG) waste samples used in this study were collected from the production of phosphoric acid factory in Morocco. The powder was washed several times with distilled water, then dried overnight in oven and sieved with 50 µm sieve. Potassium dihydrogen phosphate (KH_2PO_4) as phosphate source, sodium hydroxide pellets for pH adjustment, and polyethylene glycol oleyl ether $C_{22}H_{44}O_3$ (Brij-93 with average Mn ~ 357) as non-ionic surfactant, were obtained from Sigma-Aldrich (Germany). Distilled water (DIW) was used for all syntheses.

2.2. HAp synthesis

The hydrothermal synthesis was performed in distilled water according to the following procedure: (i) 0.3 M solution of potassium dihydrogen phosphate was prepared by dissolving 2 g KH_2PO_4 in 50 mL H_2O at room temperature under continuous stirring; (ii) 2 g of PG was added to KH_2PO_4 solution with continuous stirring at room temperature for 30 min; (iii) the solution pH was adjusted between 5 and 11 by dropwise addition of 1 M NaOH solution; (iv) 0.003–0.01 mol of the surfactant Brij 93 was added to the mixture; (v) the obtained solutions were transferred into 120 mL Teflon lined steel autoclaves and the hydrothermal synthesis was carried out at 100, 150 and 200 °C for different holding time (i.e. 1, 2, 6 and 15 h); (vi) the synthesis products were washed several times with distilled hot water and ethanol in order to remove the side products, then the products were collected by centrifugation and dried at 70 °C for 24 h in air.

The conversion to hydroxyapatite was achieved according to the reaction below:



2.3. Characterization methods

The structural characterization was performed using a Bruker AXS D8 ADVANCE X-ray diffractometer (Bruker, Germany) equipped with a Lynx Eye 1D detector with $\text{CoK}\alpha$ radiation. This device operated in a Bragg–Brentano geometry. Data were collected between 10 and 80° 2θ, with a step time of 3 s/0.02°. The characterization of the synthesized HAp for each parameter was carried out by X-ray diffraction using a PHILIPS PW 1830 diffractometer (PHILIPS, Netherlands) with $\text{CuK}\alpha$ radiation. Data were collected in the 2θ range of 15–80°, with a step size of 0.04. Rietveld refinement was performed using the FULLPROF program [29] and profile function 7 (Thompson-Cox-Hastings pseudo-Voigt convoluted with axial divergence asymmetry function) [30]. The resolution function of the instrument was obtained from the structure

refinement of LaB_6 standard. The functional groups of raw PG and elaborated HAp were analysed by attenuated total reflection (ATR) method using Fourier transform infrared spectrometer on Bruker EQUINOX 55 (Bruker, Germany). The morphology of elaborated HAp at different surfactant dosages was studied via scanning electron microscopy (SEM) on a Zeiss Gemini Leo 1530 (Zeiss, Germany). Samples were placed on conducting carbon pads and then sputtered with a thin layer of gold to prevent sample charging. Transmission electron microscopy (TEM) characterization was performed on a TECNAI G20 STWIN (FEI, Oregon, USA) with LaB_6 electron gun, operated at 200 kV. A Gatan MS794 P CCD camera and Digital Micrograph software package were used for image recording and evaluation.

3. Results and discussion

3.1. Composition and structure of phosphogypsum waste

In the first step phosphogypsum sample was characterized by powder X-ray diffraction in order to determine the crystalline phases in the sample. The Rietveld refinement of the XRD data showed that the sample contains 56.9 wt% hemi-hydrate gypsum $\text{CaSO}_4 \cdot \frac{1}{2} \text{ H}_2\text{O}$ (I2, No. 5, $Z = 12$, $a = 12.0220(4)$, $b = 6.9312(5)$, $c = 12.6867(4)$ Å and $\beta = 90.18(1)^\circ$), 42.2 wt% anhydrous CaSO_4 (Amma, No. 63, $Z = 4$, $a = 7.0016(5)$, $b = 7.0068(3)$, $c = 6.2431(3)$ Å) and 0.9 wt% of quartz SiO_2 (P321, No. 154, $Z = 3$, $a = b = 4.8949$ and $c = 5.4361$ Å). Fig. 1 shows the observed, calculated and the difference profile for the final cycle of the structure refinement.

The results of the structure refinement were confirmed by FT-IR characterization (Fig. 2). The hemi-hydrate gypsum $\text{CaSO}_4 \cdot \frac{1}{2} \text{ H}_2\text{O}$ and anhydrous CaSO_4 are identified by absorption bands characteristic to sulfate SO_4^{2-} group such as the doublet bands at 592 and 656 cm⁻¹ associating to the asymmetrical ν_4 vibrations, the band at 1005 corresponding to asymmetrical ν_1 vibrations and the doublet at 1082 and 1112 cm⁻¹ corresponding to the asymmetrical ν_3 vibrations. The presence of water in hemi-hydrate gypsum were also confirmed by its absorption band appear at 1619 cm⁻¹ corresponding to its ν_2 vibrations and doublet bands at 3550 and 3610 cm⁻¹ corresponding to its ν_1 vibrations. The presence of hemi-hydrate calcium sulfate ($\text{CaSO}_4 \cdot \frac{1}{2} \text{ H}_2\text{O}$) as main phase in the raw PG sample is in a good agreement with previous studies [31].

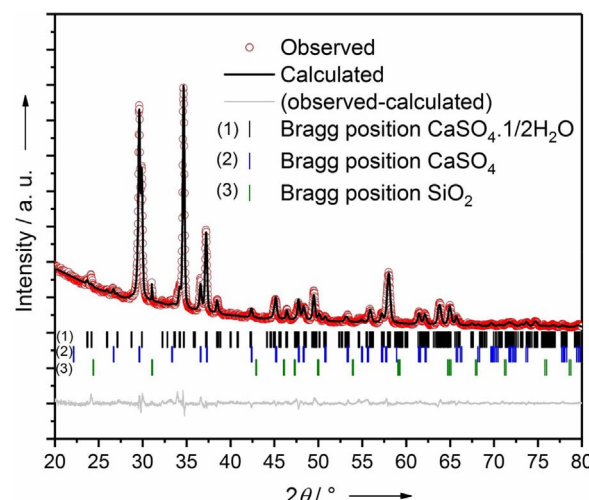


Fig. 1. Structure refinement from XRD data of phosphogypsum waste sample showing observed (red dots), calculated (black solid line) intensities and differences (grey solid line). Tick marks refer to the reflections of $\text{CaSO}_4 \cdot \frac{1}{2} \text{ H}_2\text{O}$ (1), anhydrous CaSO_4 (2) and quartz SiO_2 (3).

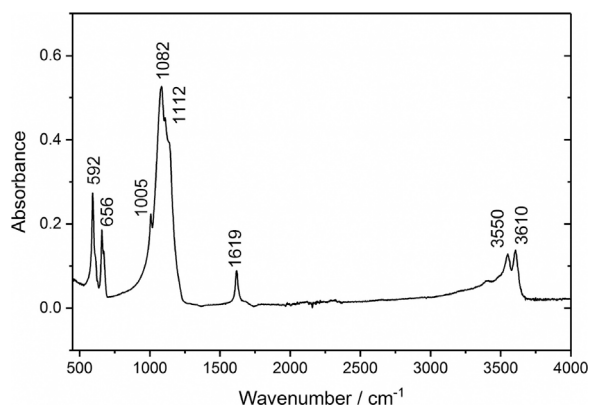


Fig. 2. ATR-FTIR spectrum of phosphogypsum waste.

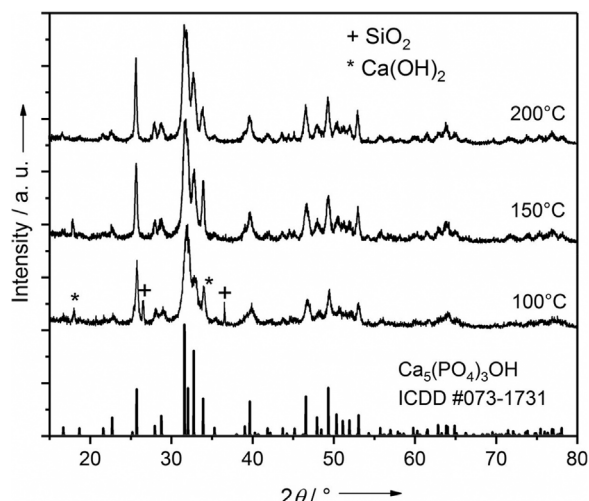


Fig. 3. XRD patterns of the materials synthesized at pH 11 at 100, 150 and 200 °C for 15 h.

3.2. Hydrothermal synthesis of hydroxyapatite

In the next step we studied the influence of temperature on the synthesis of phase pure HAp. Fig. 3 displays the XRD patterns of the materials synthesized at pH 11 at 100, 150 and 200 °C for 15 h. The XRD results reveal that nanocrystalline HAp is obtained already at 100 °C, however, with side phases (Ca(OH)₂ and quartz SiO₂), the latter was already present in the starting PG material (Fig. 1). With increasing the temperature to 150 °C, SiO₂ phase was disappeared and only Ca(OH)₂ was observed in addition to the HAp phase. The disappearance of SiO₂ can be explained by its high solubility in NaOH solution under hydrothermal conditions at temperatures above 150 °C, which it is good agreement with previous studies [32]. At 200 °C, phase pure nanocrystalline HAp was obtained, all impurity phases from the starting PG material were effectively removed being dissolved under the synthesis conditions.

The influence of synthesis time and pH were also studied. Fig. 4a shows the XRD patterns of the specimens synthesized at 200 °C and pH 11 for different synthesis times. Fig. 4b shows the XRD patterns of the specimens synthesized at 200 °C for 15 h at different pH. All the reflections in Fig. 4a can be assigned to either HAp or Ca(OH)₂ phase. The reflections corresponding to Ca(OH)₂ phase were found to decrease with increasing synthesis time, thus after 15 h only HAp phase was observed. On the other hand, CaSO₄ phase was detected in addition to HAp when the pH decreased from 11 to 5 when the synthesis was performed at 200 °C for 15 h (Fig. 4b). These results suggest that the hydrothermal conversion of PG into HAp at 200 °C and pH 11 for 15 h

takes place in two steps; (i) the complete hydrolysis of CaSO₄ into Ca(OH)₂ phase and then (ii) the reaction of formed Ca(OH)₂ with free PO₄³⁻ anions in the solution. Therefore, at low pH (≤ 9) CaSO₄ phase was observed in XRD patterns because there are no sufficient free hydroxide ions in the solution to hydrolyze all CaSO₄ in PG. As the concentration of hydroxide ions increases in the solution at pH 11, all CaSO₄ in PG transformed to Ca(OH)₂ phase (Fig. 4a). However, the second step, which involves conversion of formed Ca(OH)₂ phase into HAp, is time dependent and 15 h is required for complete reaction.

To confirm the crystal structure of HAp and to determine the unit cell parameters, Rietveld refinements of the XRD data were performed. Fig. 5 shows the observed, calculated and the difference profile for the final cycle of the structure refinement of HAp sample synthesized at 200 °C and pH 11 for 15 h. The using of sphere model with isotropic peak broadening for all XRD reflections in the first refinement attempts resulted in bad fitting (convergence factors $R_{wp} = 16.5\%$) as shown in Fig. 5a. Close inspection of the fitted XRD pattern revealed that the width of all $00l$ reflections being significantly narrower, which suggests preferential crystalline growth along the c direction. This result is consistent with the rod-like crystals as seen in Fig. 8 and Fig. 9. The using of needle-like coherent domains for Rietveld refinement gave better fittings (convergence factors $R_{wp} = 14.12\%$). The determined structural parameters (space group $P6_3/m$, No. 176, $Z = 2$, $a = b = 9.4073(6)$ and $c = 6.8895(5)$) from the structure refinements in this work were found in good agreement with previously reported values [27], which confirms the formation of stoichiometric hydroxyapatite under the present experimental conditions.

3.3. HAp nanorods synthesized with Brij-93 surfactant

In the next step, we investigated the influence of Brij-93 surfactant on the crystallization and morphology of the HAp crystals. Fig. 6 displays the XRD patterns of hydrothermally synthesized samples without and with different concentration of Brij-93 surfactant (0.003, 0.006, and 0.01 mol) at pH 11 and 200 °C for 15 h. Although all the reflections in the XRD patterns of the four samples could be indexed to the hexagonal structure of HAp, the intensities and width of $00l$ reflections are varied for the four samples. This result indicates that the crystallites size along the c direction in the three samples are different. This is also consistent with previous studies about hydrothermally synthesized hexagonal HAp rods, which were grown along the c axis [22]. These $00l$ reflections were found more intense and narrow for the samples synthesized with Brij-93 surfactant which indicates the increase in the crystallite size of HAp. The influence of Brij-93 surfactant on the crystal size of HAp nanorods were further confirmed by TEM characterizations (Fig. 9) and discussed in details below.

To confirm the removal of surfactant residues after hydrothermal synthesis, all samples were characterized by FTIR spectroscopy (Fig. 7). As can be seen from Fig. 7b–e, the absorption bands appearing at 560 and 602 cm⁻¹ corresponds to ν_4 mode of phosphate group (PO₄³⁻), while the band at 960 cm⁻¹ is due to its ν_1 mode. The two strong bands at 1022 and 1095 cm⁻¹ are also assigned to ν_3 mode of phosphate group. The weak absorption bands at 723, 865 and doublet at 1410 and 1456 cm⁻¹ correspond to ν_4 , ν_2 and ν_3 modes of CO₃²⁻, respectively [33]. The observation of these characteristic bands indicates the partial substitution of PO₄³⁻ group in HAp lattice by CO₃²⁻ group, which is due to the entrapment of atmospheric carbon dioxide during preparation [34,35]. The presence of carbonates in the prepared HAp may indicate their high biocompatibility as HAp present in human bone has 4–6 wt% carbonates [36]. The broad band at 3100–3500 could be assigned to adsorbed water, while the weak band at 3540 corresponds to the stretching vibration of OH⁻ group in the HAp lattice. For Brij-93 (Fig. 7a), characteristic absorption bands at 2900 and 1100 cm⁻¹ are attributed to C–H and C–O stretching vibrations. These absorption bands were not observed in the spectra of HAp (Fig. 7b–e), which indicates that Brij-93 is discarded during the washing process with hot water and ethanol.

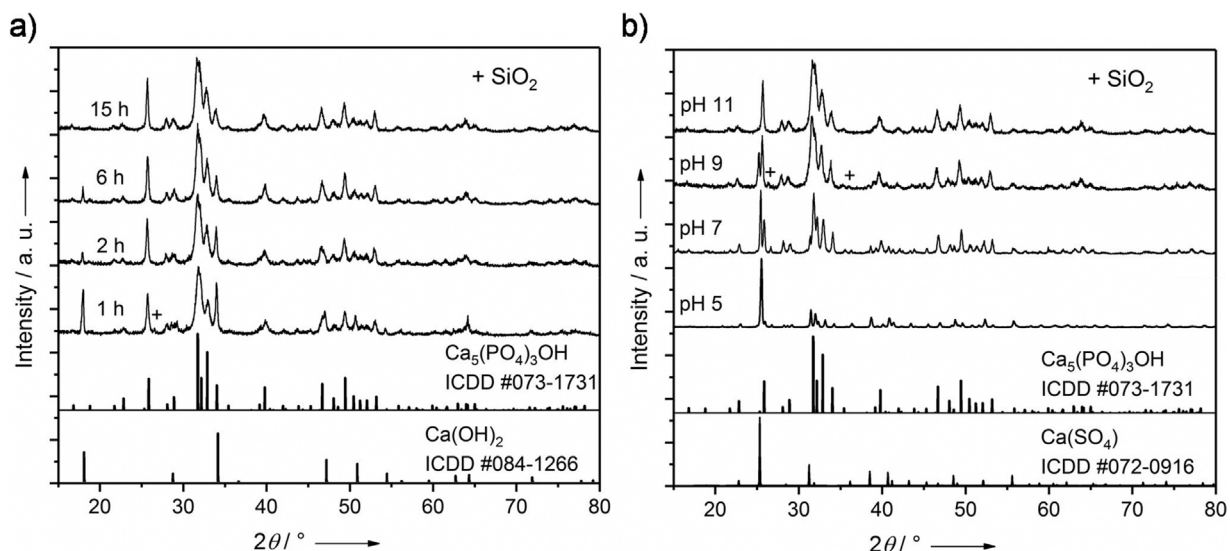


Fig. 4. XRD patterns of the materials synthesized at 200 °C: (a) at constant pH 11 and for times between 1 and 15 h; (b) at constant time (15 h) and pH between 5 and 11.

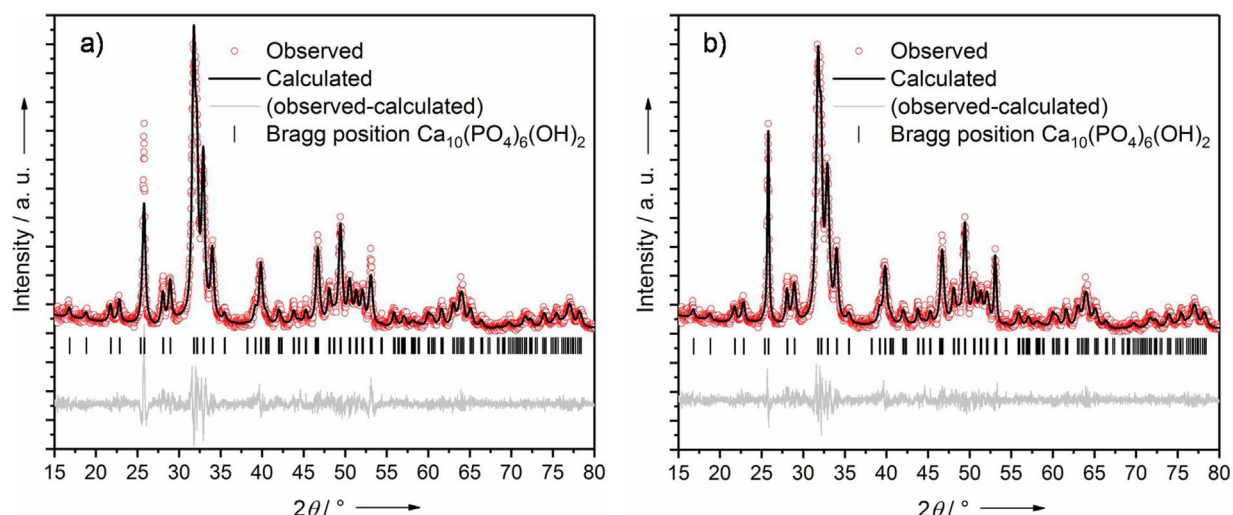


Fig. 5. Structure refinement from XRD data of HAp sample, hydrothermally synthesized at 200 °C, pH 11 for 15 h, using a single-phase model (a) with isotropic peak widths for all reflections and (b) with anisotropic peak broadening for all $00l$ reflections. Observed (red dots), calculated (black solid line) intensities and differences (grey solid line) are shown. Tick marks refer to the reflections of HAp.

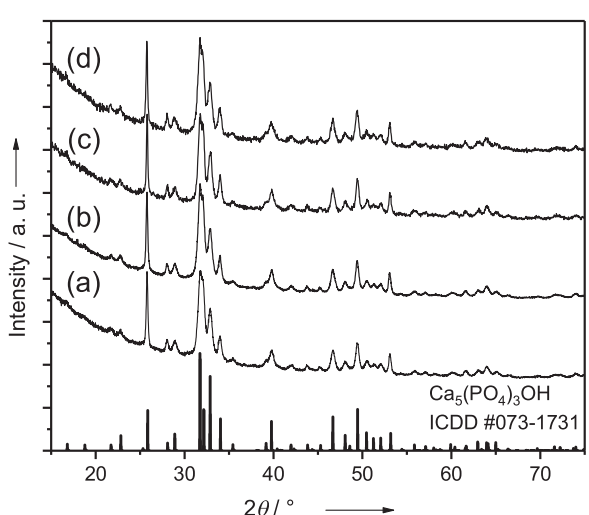


Fig. 6. XRD patterns of materials synthesized at pH 11 and 200 °C for 15 h without (a) and with 0.003 (b), 0.006 (c) and 0.01 (d) mol of Brij-93 surfactant.

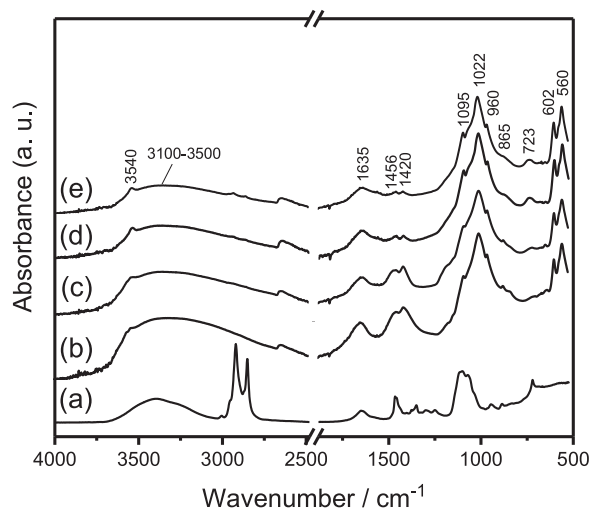


Fig. 7. FTIR spectra of Brij-93 surfactant (a) and the materials synthesized at pH 11 and 200 °C for 15 h without (b) and with 0.003 (c), 0.006 (d) and 0.01 (e) mol of Brij-93 surfactant.

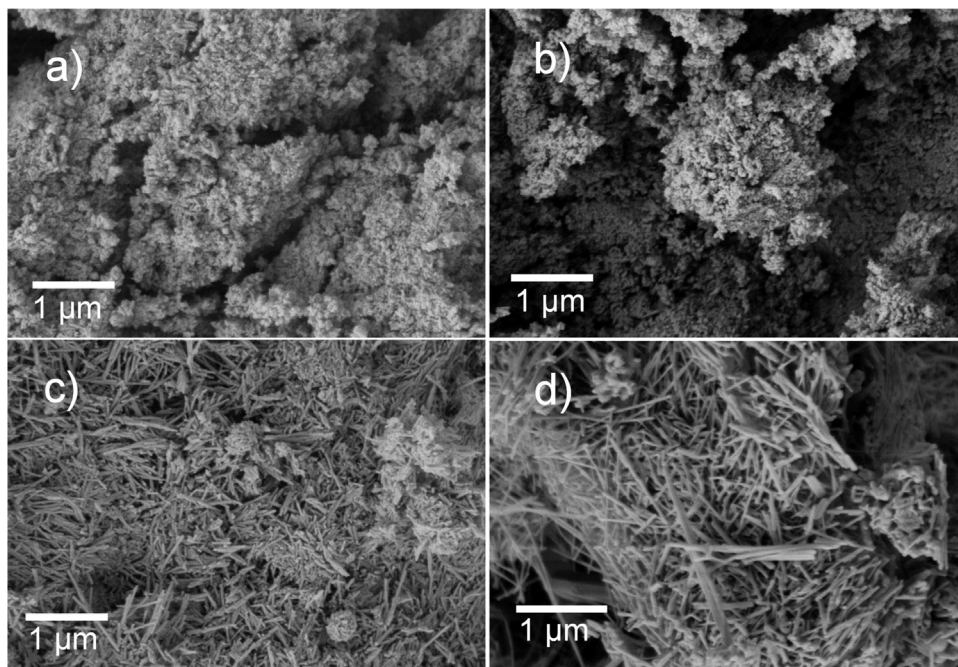


Fig. 8. SEM micrographs of HAp materials synthesized at 200 °C and pH 11 for 15 h without (a) and with 0.003 (b), 0.006 (c) and 0.01 (d) mol of Brij-93 surfactant.

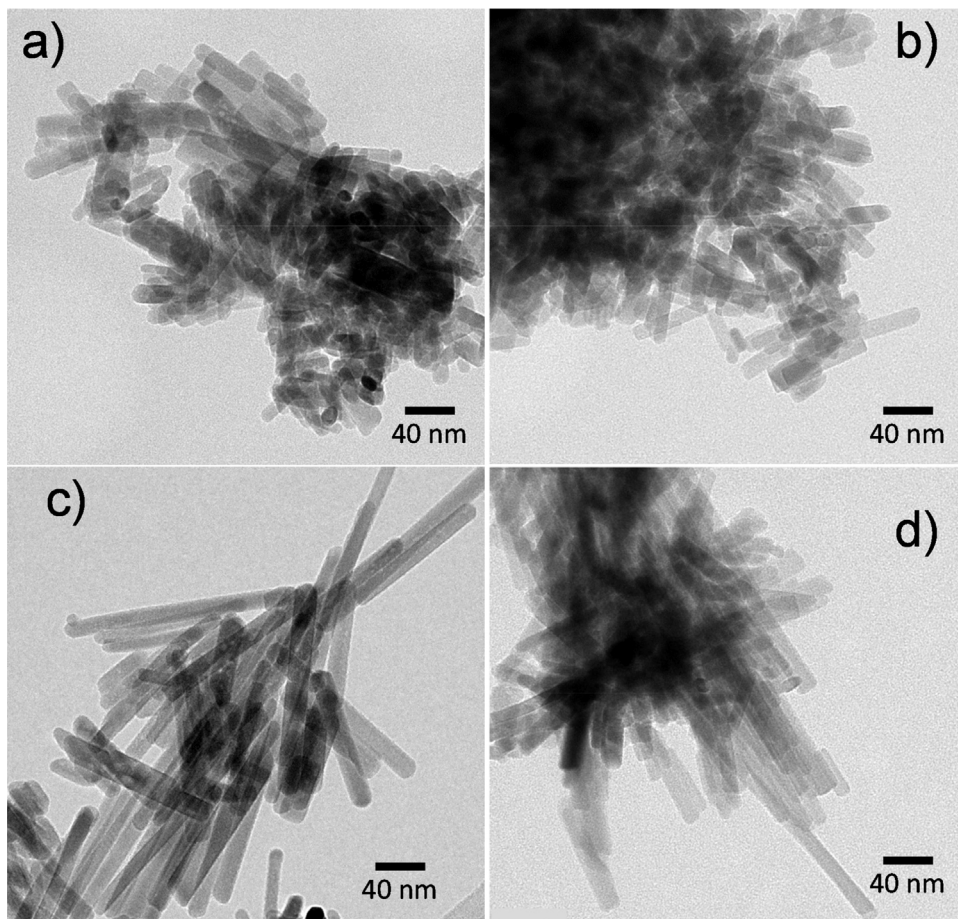


Fig. 9. TEM micrographs of HAp materials synthesized at 200 °C and pH 11 for 15 h without (a) and with 0.003 (b), 0.006 (c) and 0.01 (d) mol of Brij-93 surfactant.

The influence of Brij-93 surfactant on the morphology of synthesized HAp particles was further investigated by SEM (Fig. 8a–d) and TEM (Fig. 9a–d) inspection. As shown in Fig. 8a–d and Fig. 9a–d, all HAp materials consist of uniform rod-like particles with different aspect ratio (i.e. particle length/particle diameter). The HAp nanorods

synthesized without Brij-93 surfactant (Fig. 8a and Fig. 9a) are smaller and highly agglomerated in comparison with those synthesized with the surfactant (Fig. 8b–d); they have small aspect ratio of 3.5, where the crystal diameter and length are 18 and 63 nm, respectively. The Brij surfactant leads to an increase in the aspect ratio of HAp nanocrystals

(Fig. 9b–d), finally resulting in nanorods with aspect ratio about 10–13 and the mean size around 200–205 × 16–20 nm (Fig. 9c–d). Similar effect was observed previously in the synthesis of Co–B–N–H nanowires with Brij surfactant and was attributed to in which the Brij was chemically capped at the surface of the growth particles acting as an assembly director leading to the preferential growth in one direction preventing simultaneously the agglomeration of nanorods [37].

4. Conclusion

Nanocrystalline hydroxyapatite (HAp) was successfully synthesized from industrial waste phosphogypsum (PG) and potassium dihydrogen phosphate KH_2PO_4 by hydrothermal method. The purity and morphology of prepared HAp strongly depends on the conditions of hydrothermal synthesis. XRD data reveal that phase-pure HAp is hydrothermally obtainable in strong alkaline medium (i.e. pH = 11) at 200 °C after sufficient long time (15 h). SEM and TEM characterizations showed that the prepared HAp consists of uniform rod-like nanoparticles with different aspect ratios depending on the concentration of the Brij-93 surfactant used in the synthesis. The Brij-93 surfactant capped at the surface of the HAp crystals leads to the preferential growth in one direction preventing simultaneously the agglomeration of nanorods.

Acknowledgment

The financial support by the Otto Bayer Fellowship, application number: F-2017-BS-0121 is greatly acknowledged. This publication reflects the views only of the author, and the Commission cannot be held responsible for any use, which may be made of the information contained therein. We thank Dr. Franziska Schmidt for SEM and Sören Selve for TEM characterization.

References

- [1] T.Z. Guo, R.F. Malone, K.A. Rusch, Stabilized phosphogypsum: class C fly ash: Portland type II cement composites for potential marine application, *Environ. Sci. Technol.* 35 (2001) 3967–3973.
- [2] H. Tayibi, M. Choura, F.A. Lopez, F.J. Alguacil, A. Lopez-Delgado, Environmental impact and management of phosphogypsum, *J. Environ. Manage.* 90 (2009) 2377–2386.
- [3] J.K. Yang, W.C. Liu, L.L. Zhang, B. Xiao, Preparation of load-bearing building materials from autoclaved phosphogypsum, *Constr. Build. Mater.* 23 (2009) 687–693.
- [4] N. Degirmenci, Utilization of phosphogypsum as raw and calcined material in manufacturing of building products, *Constr. Build. Mater.* 22 (2008) 1857–1862.
- [5] C. Papastefanou, S. Stoulos, A. Ioannidou, A. Manolopoulou, The application of phosphogypsum in agriculture and the radiological impact, *J. Environ. Radioact.* 89 (2006) 188–198.
- [6] N. Degirmenci, A. Okucu, A. Turabi, Application of phosphogypsum in soil stabilization, *Build. Environ.* 42 (2007) 3393–3398.
- [7] M. Jarcho, C.H. Bolen, M.B. Thomas, J. Bobick, J.F. Kay, R.H. Doremus, Hydroxylapatite synthesis and characterization in dense polycrystalline form, *J. Mater. Sci.* 11 (1976) 2027–2035.
- [8] H. Zhou, J. Lee, Nanoscale hydroxyapatite particles for bone tissue engineering, *Acta Biomater.* 7 (2011) 2769–2781.
- [9] J.W. Jaworski, S. Cho, Y. Kim, J.H. Jung, H.S. Jeon, B.K. Min, K.Y. Kwon, Hydroxyapatite supported cobalt catalysts for hydrogen generation, *J. Colloid Interf. Sci.* 394 (2013) 401–408.
- [10] N. Razavi, B. Akhlaghinia, Hydroxyapatite nanoparticles (HAP NPs): a green and efficient heterogeneous catalyst for three-component one-pot synthesis of 2,3-dihydroquinazolin-4(1H)-one derivatives in aqueous media, *New J. Chem.* 40 (2016) 447–457.
- [11] J. Xu, T. White, P. Li, C.H. He, Y.F. Han, Hydroxyapatite foam as a catalyst for formaldehyde combustion at room temperature, *J. Am. Chem. Soc.* 132 (2010) 13172–13173.
- [12] M. Zahouily, Y. Abrouki, B. Bahlaouan, A. Rayadhi, S. Sebt, Hydroxyapatite: new efficient catalyst for the Michael addition, *Catal. Commun.* 4 (2003) 521–524.
- [13] K. Mori, T. Hara, T. Mizugaki, K. Ebihara, K. Kaneda, Hydroxyapatite-supported palladium nanoclusters: a highly active heterogeneous catalyst for selective oxidation of alcohols by use of molecular oxygen, *J. Am. Chem. Soc.* 126 (2004) 10657–10666.
- [14] A. Venugopal, M.S. Scurrell, Hydroxyapatite as a novel support for gold and ruthenium catalysts—behaviour in the water gas shift reaction, *Appl. Catal. A-Gen.* 245 (2003) 137–147.
- [15] Y.Y. Li, X.H. Lv, D. Wu, H.M. Ma, R. Feng, Y.L. Wang, B. Du, Q. Wei, Screen printed biosensor for hydrogen peroxide based on prussian blue modified hydroxyapatite, *J. Inorg. Organomet. Polym.* 23 (2013) 917–922.
- [16] L.M. Lu, L. Zhang, X.B. Zhang, S.Y. Huan, G.L. Shen, R.Q. Yu, A novel tyrosinase biosensor based on hydroxyapatite-chitosan nanocomposite for the detection of phenolic compounds, *Anal. Chim. Acta* 665 (2010) 146–151.
- [17] S.P. Wang, Y. Lei, Y. Zhang, J. Tang, G.L. Shen, R.Q. Yu, Hydroxyapatite nanoarray-based cyanide biosensor, *Anal. Biochem.* 398 (2010) 191–197.
- [18] V.E. Badillo-Almaraz, J.A. Flores, H. Arriola, F.A. Lopez, L. Ruiz-Ramirez, Elimination of fluoride ions in water for human consumption using hydroxyapatite as an adsorbent, *J. Radioanal. Nucl. Chem.* 271 (2007) 741–744.
- [19] Y.A. Feng, J.L. Gong, G.M. Zeng, Q.Y. Niu, H.Y. Zhang, C.G. Niu, J.H. Deng, M. Yan, Adsorption of Cd (II) and Zn (II) from aqueous solutions using magnetic hydroxyapatite nanoparticles as adsorbents, *Chem. Eng. J.* 162 (2010) 487–494.
- [20] C. Srilakshmi, R. Saraf, Ag-doped hydroxyapatite as efficient adsorbent for removal of Congo red dye from aqueous solution: synthesis, kinetic and equilibrium adsorption isotherm analysis, *Micropor. Mesopor. Mater.* 219 (2016) 134–144.
- [21] E. Hasret, M. Ipekoglu, S. Altintas, N.A. Ipekoglu, Microwave-assisted synthesis of hydroxyapatite for the removal of lead(II) from aqueous solutions, *Environ. Sci. Pollut. Res.* 19 (2012) 2766–2775.
- [22] Y.J. Wang, S.H. Zhang, K. Wei, N.R. Zhao, J.D. Chen, X.D. Wang, Hydrothermal synthesis of hydroxyapatite nanopowders using cationic surfactant as a template, *Mater. Lett.* 60 (2006) 1484–1487.
- [23] B. Kerebel, G. Daclusi, L.M. Kerebel, Ultrastructural studies of enamel crystallites, *J. Dent. Res.* 58 (1979) 844–851.
- [24] L.J. Wang, X.Y. Guan, H.Y. Yin, J. Moradian-Oldak, G.H. Nancollas, Mimicking the self-organized microstructure of tooth enamel, *J. Phys. Chem. C* 112 (2008) 5892–5899.
- [25] I.H. Arita, V.M. Castano, D.S. Wilkinson, Synthesis and processing of hydroxyapatite ceramic tapes with controlled porosity, *J. Mater. Sci. Mater. Med.* 6 (1995) 19–23.
- [26] U. Vijayalakshmi, S. Rajeswari, Influence of process parameters on the sol-gel synthesis of nano hydroxyapatite using various phosphorus precursors, *J. Sol-Gel Sci. Technol.* 63 (2012) 45–55.
- [27] Y. Fujishiro, H. Yabuki, K. Kawamura, T. Sato, A. Okuwaki, Preparation of needle-like hydroxyapatite by homogeneous precipitation under hydrothermal conditions, *J. Chem. Technol. Biotechnol.* 57 (1993) 349–353.
- [28] M.S. Bakshi, How surfactants control crystal growth of nanomaterials, *Cryst. Growth Des.* 16 (2016) 1104–1133.
- [29] J. Rodriguez-Carvajal, Fullprof: a program for Rietveld refinement and pattern matching analysis, *Collected Abstract of Powder Diffraction Meeting*, Toulouse, France, 1990.
- [30] L.W. Finger, D.E. Cox, A.P. Jephcoat, A correction for powder diffraction peak asymmetry due to axial divergence, *J. Appl. Crystallogr.* 27 (1994) 892–900.
- [31] N. Barka, A. Assabbane, A. Nounah, L. Laanab, Y.A. Ichou, Removal of textile dyes from aqueous solutions by natural phosphate as a new adsorbent, *Desalination* 235 (2009) 264–275.
- [32] D.A. Crerar, G.M. Anderson, Solubility and solvation reactions of quartz in dilute hydrothermal solutions, *Chem. Geol.* 8 (1971) 107–122.
- [33] S. Gunasekaran, G. Anbalagan, S. Pandi, Raman and infrared spectra of carbonates of calcite structure, *J. Raman Spectrosc.* 37 (2006) 892–899.
- [34] T.A. Kuriakose, S.N. Kalkura, M. Palanichamy, D. Arivuoli, K. Dierks, G. Bocelli, C. Betzel, Synthesis of stoichiometric nano crystalline hydroxyapatite by ethanol-based sol-gel technique at low temperature, *J. Cryst. Growth* 263 (2004) 517–523.
- [35] Z.H. Cheng, A. Yasukawa, K. Kandori, T. Ishikawa, FTIR study of adsorption of CO₂ on nonstoichiometric calcium hydroxyapatite, *Langmuir* 14 (1998) 6681–6686.
- [36] D.K. Lee, J.Y. Park, M.R. Kim, D.J. Jang, Facile hydrothermal fabrication of hollow hexagonal hydroxyapatite prisms, *CrystEngComm* 13 (2011) 5455–5459.
- [37] F. Yang, Y.Z. Li, W. Chu, C. Li, D.G. Tong, Mesoporous Co-B-N-H nanowires: superior catalysts for decomposition of hydrous hydrazine to generate hydrogen, *Catal. Sci. Technol.* 4 (2014) 3168–3179.